Electronic Supplementary Information (ESI) for

Ammonium Acetate-Modulated Gel Electrolyte Induces Uniform Zinc Deposition for Long-Cycling Zinc-Ion Hybrid Supercapacitors

Chunjiang Jin[a*], Xinglei He[a], Changwang Pan[a], Congcong Yang[b*], Wentong Chen[a*]

[a] *Jiangxi Key Laboratory of Special Functional Photoelectric Artificial Crystal Materials, School of Chemistry and Chemical Engineering, Jinggangshan University, Ji'an, Jiangxi 343009, China*

[b] *College of Chemistry and Chemical Engineering, Tarim University, Alar 843300, China*

* Correspondence authors.

E-mail addresses: jinchunjiang@jgsu.edu.cn (C. Jin), yangcc@taru.edu.cn (C. Yang), chenwentong@jgsu.edu.cn (W. Chen).

1. Experimental section

1.1 Chemical reagents and materials

Acrylamide (AM), Ammonium acetate (AAT), Zinc sulfate heptahydrate ($ZnSO_4·7H_2O$), *N,N*'-methylenebisacrylamide (MBAA), and Ammonium persulfate (APS) were produced by Sigma-Aldrich Co., Ltd. Zinc sheets were provided by Qingyuan Metal Co., Ltd.

1.2 Preparation of hydrogel electrolytes

Firstly, 2 g AM monomer was dissolved in 10 mL hot deionized water (60 ℃), followed by dissolving 3.9 g AAT and 2.88 g of $ZnSO_4·7H_2O$ under stirring. After cooling for 1 h, 0.06 g APS (as the initiator) and 0.006 g MBAA (as the crosslinker) were added to the above solution and stirred for 10 min. Then the resulting mixture was ultrasonicated for 10 min to preliminarily remove bubbles. Finally, the clear liquid was transferred to a glass mold and thermally polymerized at 60 ℃ for 90 min to obtain the $ZnSO_4$-contained polyacrylamide (PAM)/AAT hydrogel electrolyte, labeled as PAAHE. As a comparison, the $ZnSO_4$-contained PAM hydrogel electrolyte (denoted as PAHE) was synthesized using the same preparation method without AAT.

1.3 Preparation of coal pitch-based activated carbon material

Coal tar pitch derived porous carbon material (CPC) was prepared by the one-step carbonization/activation method. Firstly, the coal tar pitch and KOH was mixed in a 1:4 mass ratio. Afterwards, the mixture was carbonized and activated at 800 ℃ for 2 h in an Ar atmosphere, with a heating rate of 5 ℃ min^{-1}. The product was repeatedly washed with dilute hydrochloric acid solution and deionized water and then dried at 80 ℃ for 24 h to finally obtain CPC.

1.4 Material characterization

The Fourier transform infrared (FTIR, VERTEX 70 RAMI) spectroscopies were

used to investigate the structure of hydrogel electrolytes. The tensile and compression tests were conducted by securing the hydrogel electrolytes to two clamps with a tensile testing machine (ZQ-990LB). The tensile tests were executed on specimens measuring 20.0×10.0×1.5 mm at a rate of 150 mm min^{-1}. The compression tests were performed on cylinders with a diameter of 12 mm and a height of 25 mm. The morphology, structure, and components of hydrogel electrolytes, CPC and cycled Zn foils were studied by scanning electron microscope (SEM, JEM-2100). The surface texture of Zn electrodes cycled in hydrogel electrolytes was analyzed by XRD (Bruker D8 Advance).

1.5 Electrode preparation and device assembly

Zn-ion hybrid capacitors (ZHCs): The AC cathode was prepared by mixing AC, acetylene black, and polytetrafluoroethylene with a mass ratio of 8:1:1, dispersed in 5 mL of anhydrous ethanol by ultrasonication, dried at 70 ℃, and cut into round sheets (a mass of 2 mg and an area of 1.1304 cm^2). The hydrogel electrolytes were synthesized in situ between AC cathode and Zn anode (Zn foils with 100 μm thickness, 1.1304 cm^2 area) to assemble quasi-solid-state ZHCs.

1.6 Electrochemical performance

The linear sweep voltammetry (LSV) was carried out on a CHI760E electrochemical analyzer by three-electrode configurations. The three-electrode system for LSV consisted of Ti plate working electrode, Zn counter electrode, and Ag/AgCl reference electrode. The cyclic voltammetry (CV) and electrochemical impedance spectroscopy (EIS) were conducted on an electrochemical workstation (CHI760E). EIS characterized the ionic conductivity in the frequency range of 10^{-1}–10^5 Hz, and the corresponding values were calculated by the following equation[1]:

$$\sigma = \frac{L}{AR} \tag{S1}$$

where σ represents the ionic conductivity, R (Ω) is the electrolyte resistance according to EIS measurement, L (m) represents the thickness of the hydrogel electrolyte (2.1 mm), and A (m^2) is the area of hydrogel electrolyte (1 cm^2). Zn^{2+} transference numbers ($t_{Zn^{2+}}$) were evaluated in symmetrical Zn cells combined by EIS before and after the chronoamperogram test and determined by the following equation[2]:

$$t_{Zn^{2+}} = \frac{I_s(\Delta V - I_0 R_0)}{I_0(\Delta V - I_s R_s)} \quad \text{(S2)}$$

where ΔV is the applied voltage polarization, I_s and R_s are the steady state current and resistance, respectively, and I_0 and R_0 are the initial current and resistance, respectively. The applied voltage polarization here is 10 mV.

The electrochemical impedance spectroscopy (EIS) curves of hydrogel electrolytes at different temperatures were measured and the activation energy (E_a) was further obtained according to the Arrhenius equation. The calculation equation is as follows[3]:

$$\frac{1}{R_{ct}} = A \exp\left(-\frac{E_a}{RT}\right) \quad \text{(S3)}$$

where R_{ct}, A, R, and T respectively represent the charge transfer resistance, pre-exponential factor, universal gas constant, and thermodynamic temperature, respectively. The cycling performance of Zn//Zn cells, Zn//Cu cells, Zn//I_2 cells, and ZHCs was tested on the M340A battery tester.

The cycling performance of the Zn||Zn cells and Zn||Cu cells with an electrode area of 1.1304 cm^2 was measured on a battery test system (M340A Land). Ultrathin Zn foils with a thickness of ~20 μm were used for cycling tests of Zn//Zn cells at 20 mA cm^{-2} and 10 mAh cm^{-2}. Thick Zn foils (~100 μm) were used for cycling tests of Zn//Zn (at

1 mA cm^{-2}/1 mAh cm^{-2} and 20 mA cm^{-2}/1 mAh cm^{-2}) and Zn//Cu (at 4 mA cm^{-2}/1 mAh cm^{-2}) cells.

The galvanostatic charge/discharge (GCD) and cycling tests of ZHCs were conducted on the M340A Land battery test system. The specific capacity (C, mAh cm^{-2}) and energy density (E, Wh cm^{-2}) were obtained from the M340A Land battery test system. The power density (P, W cm^{-2}) was calculated as follows[4]:

$$P = \frac{3600E}{t} \tag{S4}$$

where E (Wh cm^{-2}) represents the energy density, and t (s) is the discharging time.

2. Supplementary figures and tables

Fig. S1. Digital photo showing the successful completion of PAAHE.

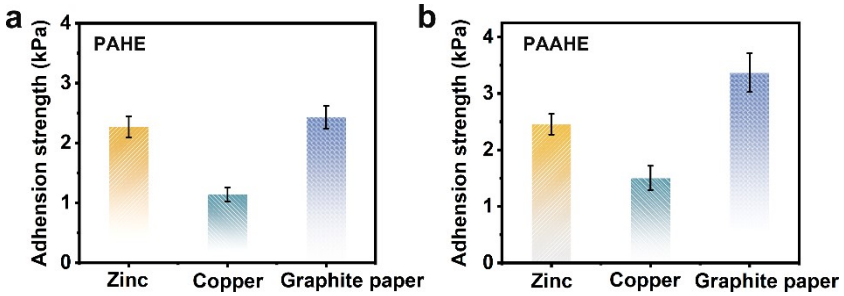

Fig. S2. Shear adhesion strengths on Cu foil, Zn foil, and graphite paper of (a) PAHE and (b) PAAHE.

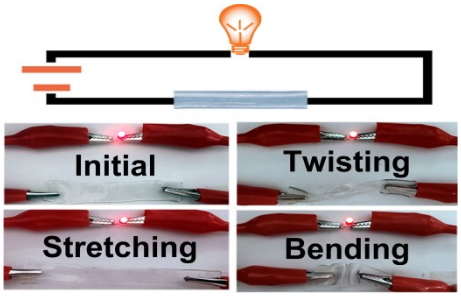

Fig. S3. Using PAAHE as conductor, the circuit schematic diagram is simulated and twisted, stretched and folded respectively.

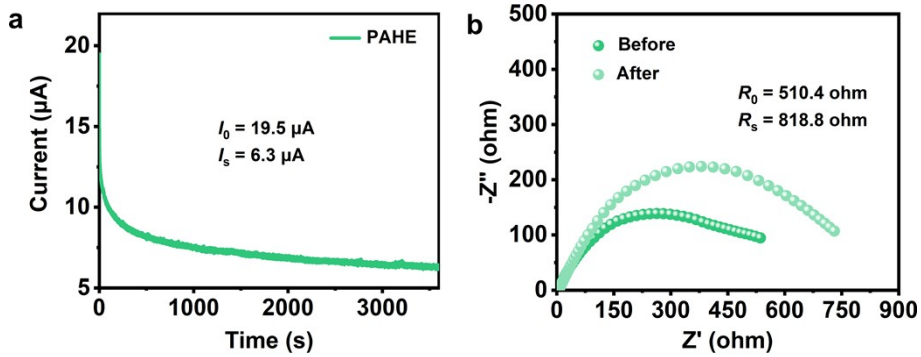

Fig. S4. (a) EIS curves of Zn//Zn symmetric cells with PAHE before and after polarization at an applied voltage of 10 mV. (b) The corresponding *I*−*t* curves of Zn//Zn symmetric cells with PAHE.

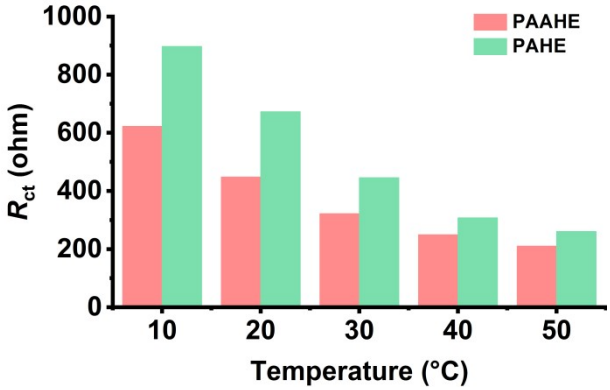

Fig. S5. *R*ct values under various temperatures in PAHE and PAAHE

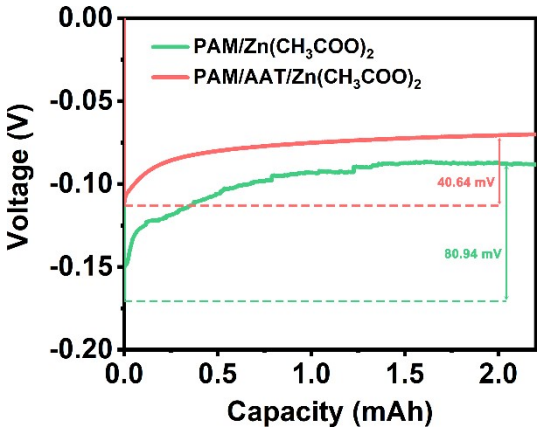

Fig. S6. NOP of Zn//Zn cells based on different electrolytes.

As shown in Figure S6, we replaced the $ZnSO_4$ electrolyte in the previously synthesized PAHE and PAAHE with a $Zn(CH_3COO)_2$ electrolyte to exclude the influence of SO_4^{2-}, and subsequently performed NOP tests. The NOP of the PAM/$Zn(CH_3COO)_2$ hydrogel electrolyte without AAT was measured to be 80.94 mV, which is significantly higher than that of the gel electrolyte incorporating AAT molecules (40.46 mV). However, its NOP value remains lower than that of PAHE, indicating that the $-COO^-$ from the zinc acetate salt itself contributes to reducing the nucleation energy barrier.

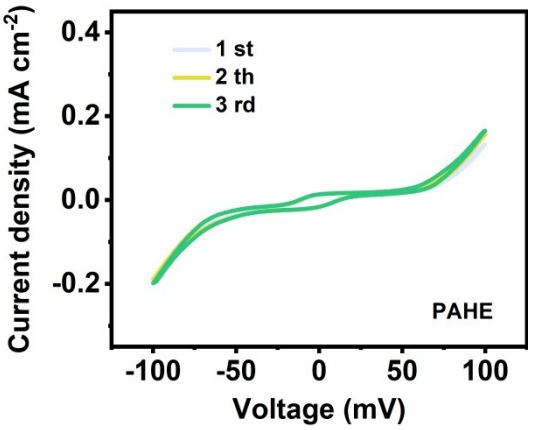

Fig. S7. CV curves of Zn//Zn cells using PAHE measured at a scan rate of 10 mV s^{-1} at the 1st, 2nd, and 3rd cycles.

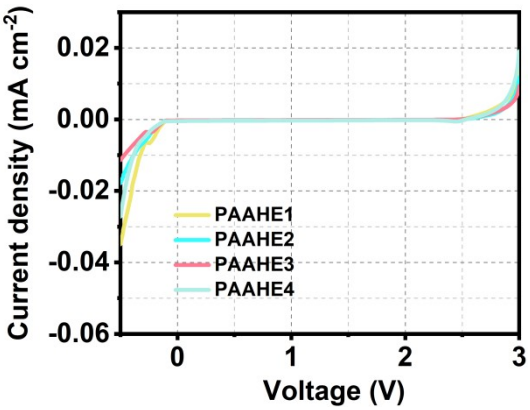

Fig. S8. LSV curves of Zn//Ti cells with PAAHE.

We have repeated the LSV measurements on multiple freshly prepared PAAHE samples (n=4) using the same Ti//Zn cell configuration. The results, now included in the Fig. S8, demonstrate excellent reproducibility, with the determined ESW consistently around 2.56 ± 0.05 V. This confirms that the result is not an artifact but a reproducible property of our material system.

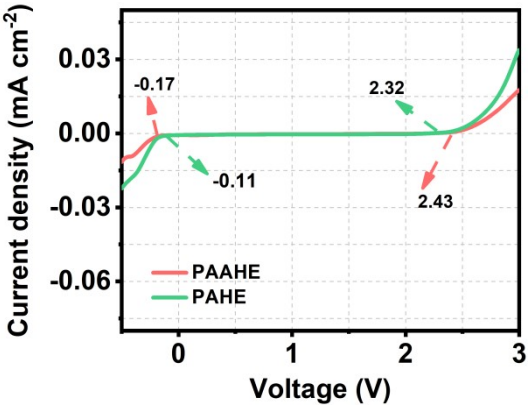

Fig. S9. LSV curves of Zn//Pt cells with PAAHE and PAHE

The LSV measurement configuration consisted of Pt (working electrode), Zn (counter electrode), and Ag/AgCl (reference electrode). The data presented in Figure S9 demonstrate that the stability window measured with the Pt electrode closely matched that obtained using the Ti electrode.

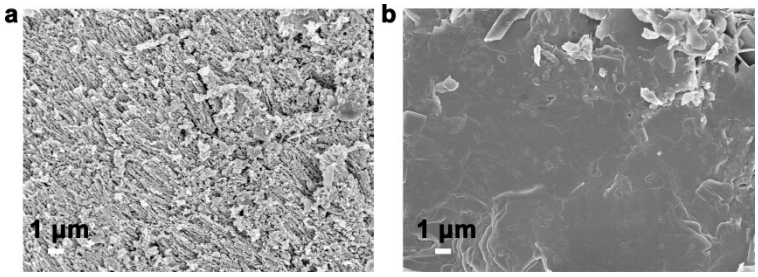

Fig. S10. SEM images of Zn foils after cycling in in (a) PAHE and (b) PAAHE.

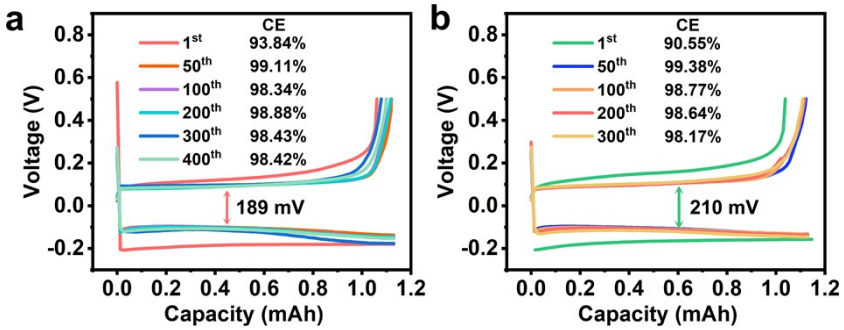

Fig. S11. GCD profiles of Zn//Cu cells with (a) PAAHE and (b) PAHE.

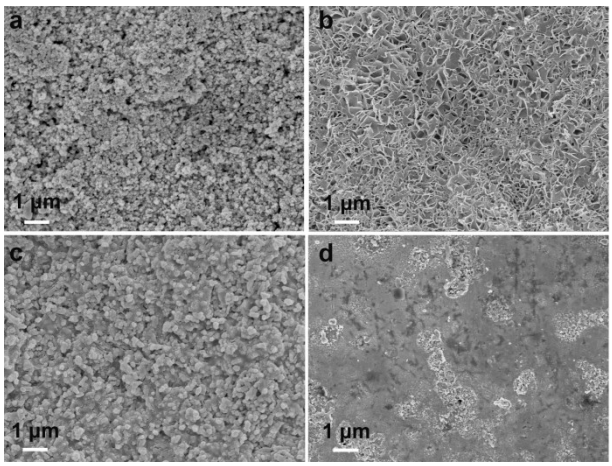

Fig. S12. SEM images of (a) Cu foil and (b) Zn foil cycled in PAHE. SEM images of (c) Cu foil and (d) Zn foil cycled in PAAHE.

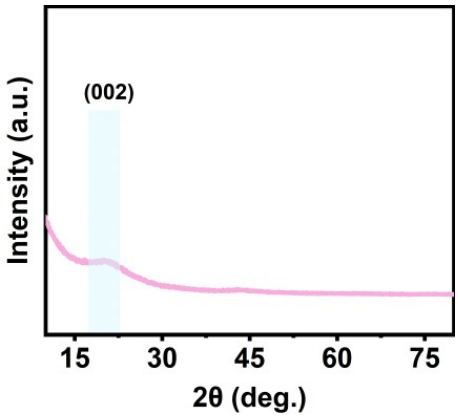

Fig. S13. XRD pattern of CPC.

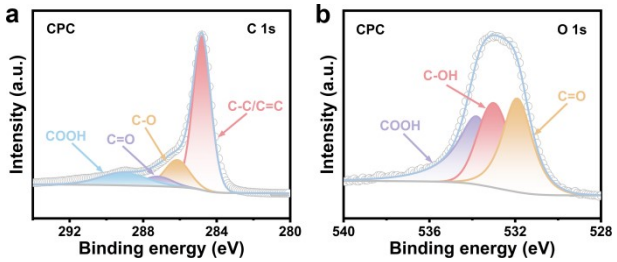

Fig. S14. (a) C 1s and (b) O 1s XPS spectra for CPC.

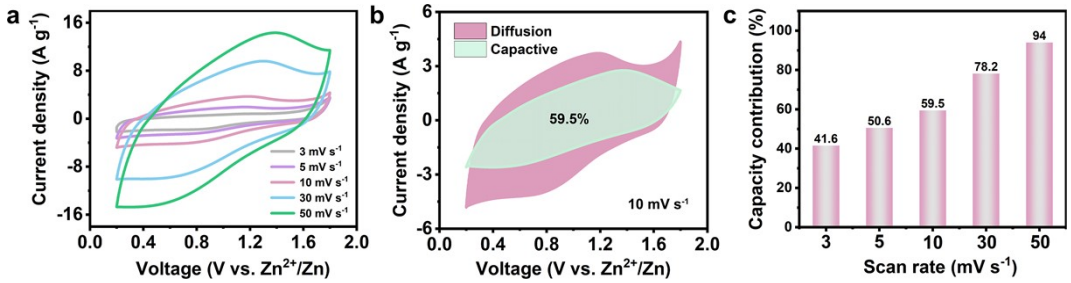

Fig. S15. (a) CV curve of Zn|PAHE|CPC ZHC. (b) Capacitance behavior contribution at 10 mV^{-1} of Zn|PAHE|CPC ZHC. (c) Capacitance behavior contribution ratio at sweep rates ranging from 3 to 50 mV^{-1} of Zn|PAHE|CPC ZHC.

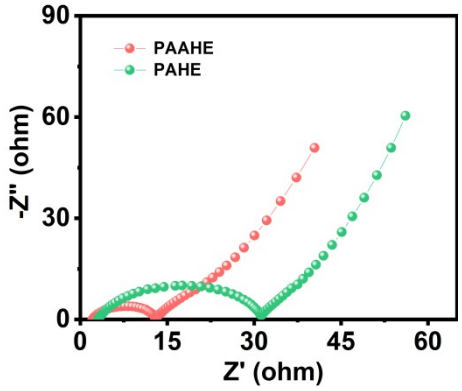

Fig. S16. Nyquist plots of ZHCs.

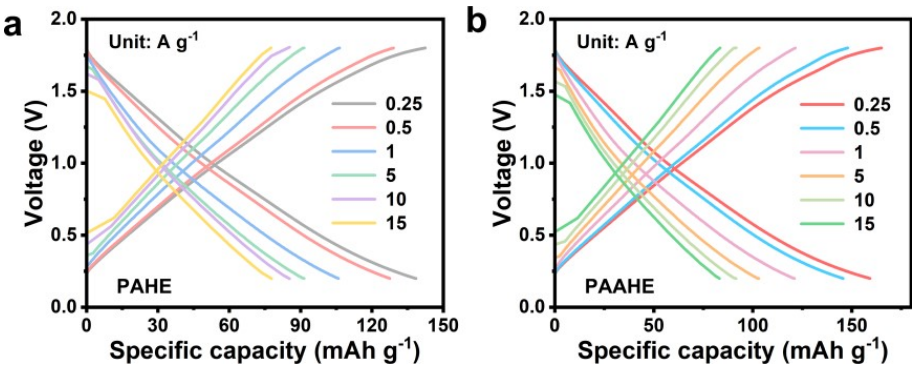

Fig. S17. GCD curves of the (a) Zn|PAHE|CPC ZHC and (b) Zn|PAAHE|CPC ZHC at

0.25−15 A g^{-1}

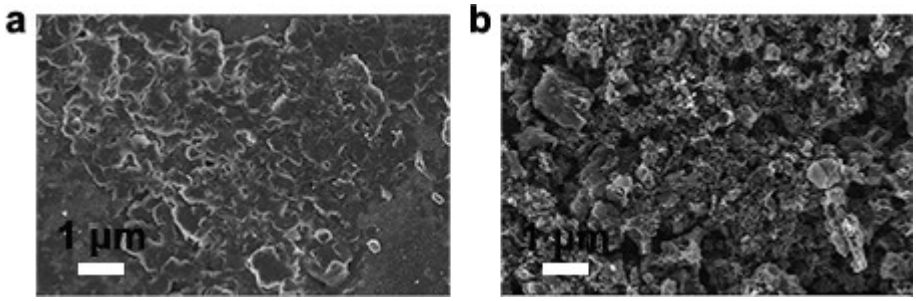

Fig. S18. SEM images of (a) Zn anode and (b) carbon electrode after cycling in Zn|PAHE|CPC ZHC.

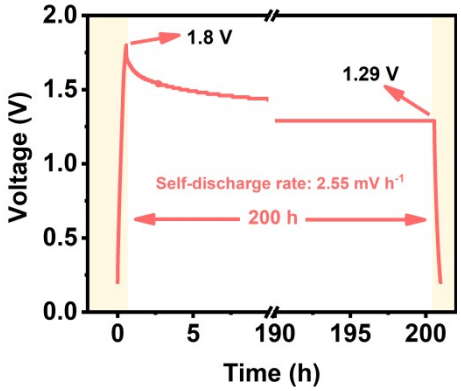

Fig. S19. Self-discharge curve of Zn|PAAHE|CPC ZHC.

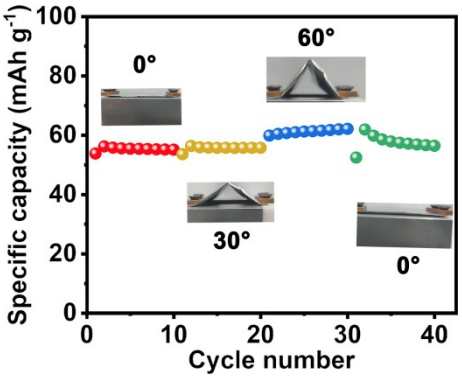

Fig. S20. Specific capacities of Zn|PAAHE|CPC ZHC at different bending angles.

Fig. S21. Digital photographs showing the application of Zn|PAAHE|CPC ZHC in the electronic timer.

Table S1. Comparison of cycle duration between our PAAHE-optimized Zn//Zn cell and reported cells.

Electrolytes	**Current density, capacity ($mA\ cm^{-2}$, $mAh\ cm^{-2}$)**	**Lifespans (h)**	**Ref.**
IL-AE	1, 1	700	5
7W1P	1, 2	600	6
Zn-ML	0.5, 0.1	140	7
PIZn	4, 2	300	8
La^{3+}-ZS	10, 5.93	140	9
PDMS/TiO_2-x	10, 10	300	10
CGPPHE	1, 1	350	11
$ZnSO_4$	2, 2	520	12
PHSHE	2, 0.5	400	13
SF-gel electrolytes.	3, 1	200	14
PAAHE	**1, 1**	**750**	**This Work**

Table S2. Comparison of Depth of discharge levels of symmetric cells.

Electrolytes	Current density, capacity (mA cm-2, mAh cm-2)	Lifespans (h)	Depth of discharge (%)	Ref.
Ag-Zn	2, 2	100	14	15
Cu Foam@Zn	2, 1	150	20.32	16
Zn@CNT/CC	5, 2.5	150	35	17
3M ZnSO4	5, 2.5	150	41.3	18
MXene	5, 1	100	3.4	19
PHSHE	5, 5	160	28.7	13
Zn@CNF	4, 4	120	40	20
100 mM DOL	1, 10	140	34.19	21
PAAHE	**10, 5**	**180**	**50.81**	**This Work**

Table S3. Comparison of CEs between our PAAHE-optimized Zn//Cu cell with reported cells.

Energy storage	**Average CE (%)**	**Cycles**	**Current density ($mA\ cm^{-2}$)**	**Ref.**
$ZnSO_4$-glucose	97.2	200	1	22
ZnSO4/15C5	98.4	300	2	23
PAA	99.53	300	5	24
D-ZS	99.5	270	5	25

P2VP	99.11	200	1	26
ZWO@Zn	99.36	180	1	27
PAAHE	**99.7**	**480**	**4**	**This Work**

Table S4 Comparison of energy/power density of Zn|PAAHE|CPC ZHC with other reported devices.

Device	Energy density (Wh kg^{-1})	Power density (W kg^{-1})	References
Zn//GPE-3//AC	66.83 Wh kg−1	187.96 W kg−1	28
NPFC700-based ZHC	60.1 Wh kg−1	74.2 W kg−1	29
CNPK-based ZHC	89.3 Wh kg−1	79.0 W kg−1	30
Zn//PAAm/agar/Zn(CF3SO3)2//NC ZHSC	61.3 Wh kg−1	209.0 W kg−1	31
Zn//PAM-*co*-PAA/k-CG/ZnSO4//NMXC ZHSC	54.9 Wh kg−1	75.8 W kg−1	32
BC-CNa//Zn ZnHS	35.9 Wh kg−1	149.6 W kg−1	33
WC-6ZnN-12U based ZHS	27.7 Wh kg−1	35.7 W kg−1	34
Zn|PAAHE|CPC ZHC	147.4 Wh kg−1	207.3 W kg−1	**This work**

References

1. Y. Guo, X. Zhu, J. Zhang, T. Zhang, Z. Wang, M. Shan, F. Wang, C. C. Cao, G. Xu and M. Zhu, *Angewandte Chemie International Edition*, 2025, **64**, e202422047.
2. Z. Peng, L. Tang, S. Li, L. Tan and Y. Chen, *Angewandte Chemie International Edition*, 2025, **64**, e202418242.
3. J. Li, H. Zhang, Z. Liu, H. Du, H. Wan, X. Li, J. Yang and C. Yan, *Advanced Functional Materials*, 2025, **35**, 2412865.
4. C. Leng, Z. Zhao, X. Wang, Y. V. Fedoseeva, L. G. Bulusheva, A. V. Okotrub, J. Xiao and J. Qiu, *ENERGY & ENVIRONMENTAL MATERIALS*, 2024, **7**, e12484.
5. L. Yu, J. Huang, S. Wang, L. Qi, S. Wang and C. Chen, *Advanced Materials*, 2023, **35**, 2210789.
6. Z. Xie, N. Chen, M. Zhang, M. Wang, X. Zheng, S. Liu, R. Luo, L. Song, Y. Meng, Z. Liu, Z. Li and W. Chen, *ACS Energy Letters*, 2024, **9**, 3380-3390.
7. F. Li, C. Zhou, J. Zhang, Y. Gao, Q. Nan, J. Luo, Z. Xu, Z. Zhao, P. Rao, J. Li, Z. Kang, X. Shi and X. Tian, *Advanced Materials*, 2024, **36**, 2408213.
8. M. Zhu, J. Hu, Q. Lu, H. Dong, D. D. Karnaushenko, C. Becker, D. Karnaushenko, Y. Li, H. Tang, Z. Qu, J. Ge and O. G. Schmidt, *Advanced Materials*, 2021, **33**, 2007497.
9. J. Manigrasso, I. Chillón, V. Genna, P. Vidossich, S. Somarowthu, A. M. Pyle, M. De Vivo and M. Marcia, *Nature Communications*, 2022, **13**, 1.
10. Z. Guo, L. Fan, C. Zhao, A. Chen, N. Liu, Y. Zhang and N. Zhang, *Advanced Materials*, 2022,

34, 2105133.
11. C. Liu, F. Guo, Q. Yang, H. Mi, C. Ji, N. Yang and J. Qiu, *Small Methods*, 2023, **7**, 2201398.
12. J. Zhang, W. Huang, L. Li, C. Chang, K. Yang, L. Gao and X. Pu, *Advanced Materials*, 2023, **35**, 2300073.
13. L. Xie, Y. Liang, Z. Wang, W. Zhang, F. Guo, X. Chang, H. Mi and J. Qiu, *ACS Applied Polymer Materials*, 2023, **5**, 10342-10351.
14. F. Mo, Y. Lu, M. Cui, Q. Liu, W. Ling, J. Zhang and W. Wang, *Journal of Electroanalytical Chemistry*, 2023, **938**, 117466.
15. Q. Lu, C. Liu, Y. Du, X. Wang, L. Ding, A. Omar and D. Mikhailova, *ACS Applied Materials & Interfaces*, 2021, **13**, 16869-16875.
16. C. Li, X. Shi, S. Liang, X. Ma, M. Han, X. Wu and J. Zhou, *Chemical Engineering Journal*, 2020, **379**, 122248.
17. Y. Zeng, X. Zhang, R. Qin, X. Liu, P. Fang, D. Zheng, Y. Tong and X. Lu, *Advanced Materials*, 2019, **31**, 1903675.
18. Z. Xu, S. Jin, N. Zhang, W. Deng, M. H. Seo and X. Wang, *Nano Letters*, 2022, **22**, 1350-1357.
19. N. Zhang, S. Huang, Z. Yuan, J. Zhu, Z. Zhao and Z. Niu, *Angewandte Chemie International Edition*, 2021, **60**, 2861-2865.
20. J. Li, Q. Lin, Z. Zheng, L. Cao, W. Lv and Y. Chen, *ACS Applied Materials & Interfaces*, 2022, **14**, 12323-12330.
21. Y. He, Z. Chen, J. Feng, J. Wang, L. Zhang, H. Gu, L. Sheng, P. Yao, F. R. Wang and Z. Hao, *Small*, 2025, **21**, 2411755.
22. P. Sun, L. Ma, W. Zhou, M. Qiu, Z. Wang, D. Chao and W. Mai, *Angewandte Chemie International Edition*, 2021, **60**, 18247-18255.
23. A. Zhou, H. Wang, X. Hu, F. Zhang, Y. Zhao, Z. Hu, Q. Zhang, Z. Song, Y. Huang, L. Li, F. Wu and R. Chen, *Science Bulletin*, 2023, **68**, 2170-2179.
24. K. Ouyang, F. Li, D. Ma, Y. Wang, S. Shen, M. Yang, J. Qiu, W. Wen, N. Zhao, H. Mi and P. Zhang, *ACS Energy Letters*, 2023, **8**, 5229-5239.
25. M. He, J. Chen, A. Hu, Z. Yan, L. Cao and J. Long, *Energy Storage Materials*, 2023, **62**, 102941.
26. X. Cai, W. Tian, Z. Zhang, Y. Sun, L. Yang, H. Mu, C. Lian and H. Qiu, *Advanced Materials*, 2024, **36**, 2307727.
27. J. Cao, H. Wu, D. Zhang, D. Luo, L. Zhang, X. Yang, J. Qin and G. He, *Angewandte Chemie International Edition*, 2024, **63**, e202319661.
28. H. Yang, J. Zhang, J. Yao, D. Zuo, J. Xu and H. Zhang, *Journal of Power Sources*, 2022, **548**, 232070.
29. F. Wei, Y. Wei, J. Wang, M. Han and Y. Lv, *Chemical Engineering Journal*, 2022, **450**, 137919.
30. H. Zhang, Z. Chen, Y. Zhang, Z. Ma, Y. Zhang, L. Bai and L. Sun, *Journal of Materials Chemistry A*, 2021, **9**, 16565-16574.
31. C. Ji, D. Wu, Z. Liu, H. Mi, Y. Liao, M. Wu, H. Cui, X. Li, T. Wu and Z. Bai, *ACS Applied Materials & Interfaces*, 2022, **14**, 23452-23464.
32. H. Cui, H. Mi, C. Ji, F. Guo, Y. Chen, D. Wu, J. Qiu and H. Xie, *Journal of Materials Chemistry A*, 2021, **9**, 23941-23954.
33. H. Chen, Y. Zheng, X. Zhu, W. Hong, Y. Tong, Y. Lu, G. Pei, Y. Pang, Z. Shen and C. Guan, *Materials Research Bulletin*, 2021, **139**, 111281.
34. G. Lou, G. Pei, Y. Wu, Y. Lu, Y. Wu, X. Zhu, Y. Pang, Z. Shen, Q. Wu, S. Fu and H. Chen, *Chemical Engineering Journal*, 2021, **413**, 127502.